Supplementary Information for:

Photodetection and Scintillation Characterizations of Novel Lead-Bismuth Double Perovskite Halides

Francesco Maddalena,[1,2,] Marcin E. Witkowski,[3] Michal Makowski,[3] Abdellah Bachiri,[3] Arramel,[4] Ting Yang,[2] Muhammad Haris Mahyuddin,[5] Matilde Baravaglio,[6] Mohamed Boutchich,[2,7,8] Winicjusz Drozdowski,[3] Christophe Dujardin,[6] Muhammad Danang Birowosuto[9,*], and Cuong Dang[1,2,*]*

[1]School of Electrical and Electronic Engineering, Nanyang Technological University, 50 Nanyang Avenue, 639798, Singapore

[2]CINTRA UMI CNRS/NTU/THALES 3288, Research Techno Plaza, 50 Nanyang Drive, Border X Block, Level 6, 637553, Singapore

[3] Institute of Physics, Faculty of Physics, Astronomy, and Informatics, Nicolaus Copernicus University in Torun, ul. Grudziadzka 5, 87-100 Torun, Poland

[4] Department of Physics, National University of Singapore, 2 Science Drive 3, Singapore 117551, Singapore

[5]Research Center for Nanoscience and Nanotechnology, Institut Teknologi Bandung, Jl. Ganesha 10, Bandung 40132, Indonesia.

[6]Universitè de Lyon, Universitè Claude Bernard, Lyon 1, CNRS, Institut Lumière Matière UMR5306, Villeurbanne F-69622, France

[7]Sorbonne Université, CNRS, Laboratoire de Génie Electrique et Electronique de Paris, 75252, Paris, France

[8]Université Paris-Saclay, CentraleSupélec, CNRS, Laboratoire de Génie Electrique et Electronique de Paris, 91192, Gif-sur-Yvette, France.

[9]Łukasiewicz Research Network-PORT Polish Center for Technology Development, Stabłowicka 147, 54-066 Wrocław, Poland

[*]Corresponding Authors.

Email: *francesco_maddalena@ntu.edu.sg; muhammad.birowosuto@port.lukasiewicz.gov.pl; hcdang@ntu.edu.sg*

KEYWORDS**:** perovskite, photodiode, X-ray, scintillator.

List of supplementary materials

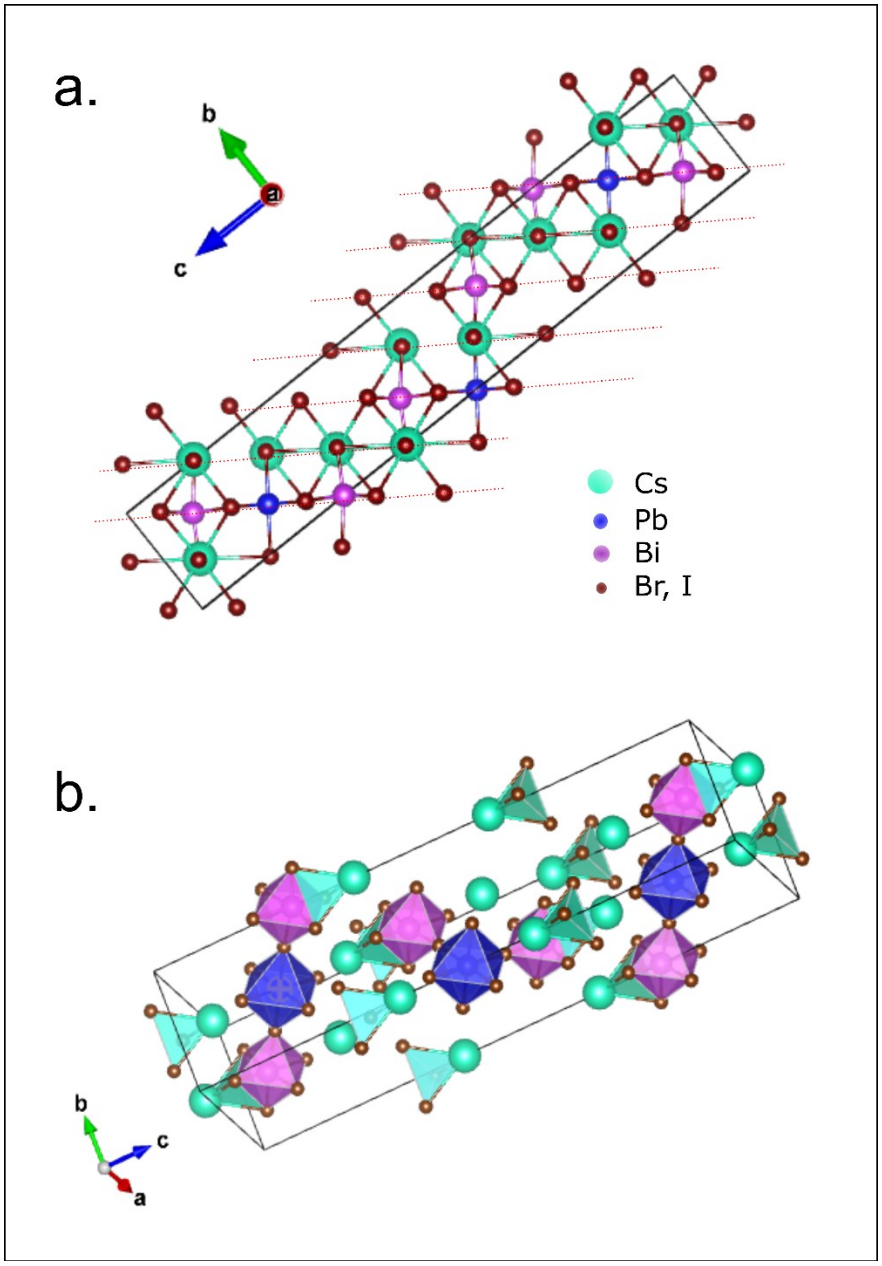

Figure S1. Crystal structure of the $Cs_4PbBi_2X_{12}$ double perovskite from different perspectives, a) highlighting the layered structure of the material and b) highlighting the PbX_6 and BiX_6 octahedra structure.

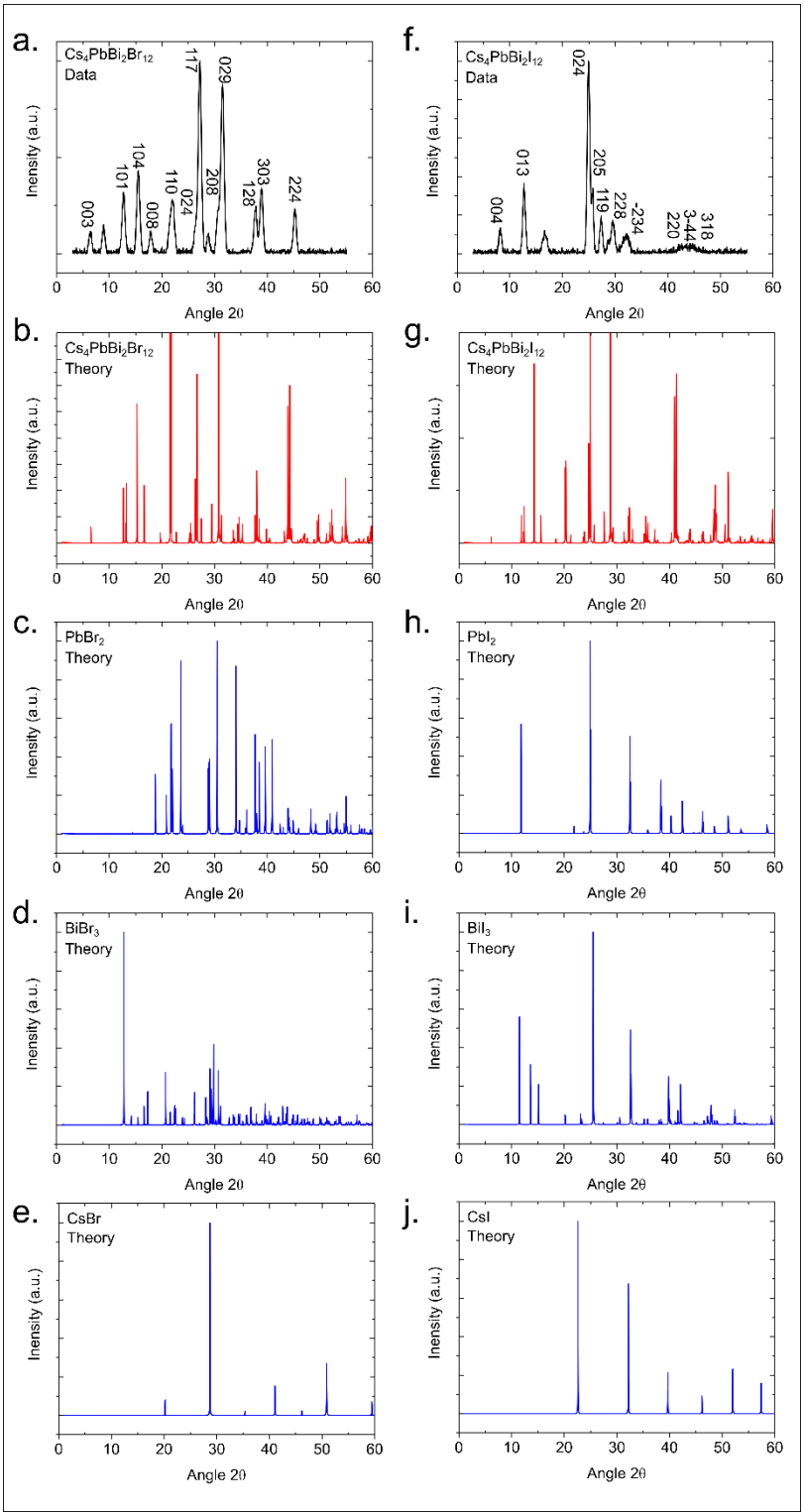

Figure S2. Diffractograms for the $Cs_4PbBi_2X_{12}$ double perovskites and their precursors. a) $Cs_4PbBi_2Br_{12}$ (Data), $Cs_4PbBi_2Br_{12}$ (Data), b) $Cs_4PbBi_2Br_{12}$ (Theory, trigonal structure), c) $PbBr_2$, d) $BiBr_3$, e) CsBr, f) $Cs_4PbBi_2I_{12}$ (Data), g) $Cs_4PbBi_2I_{12}$ (Theory, trigonal structure), h) PbI_2, i) BiI_3, and j) CsI.

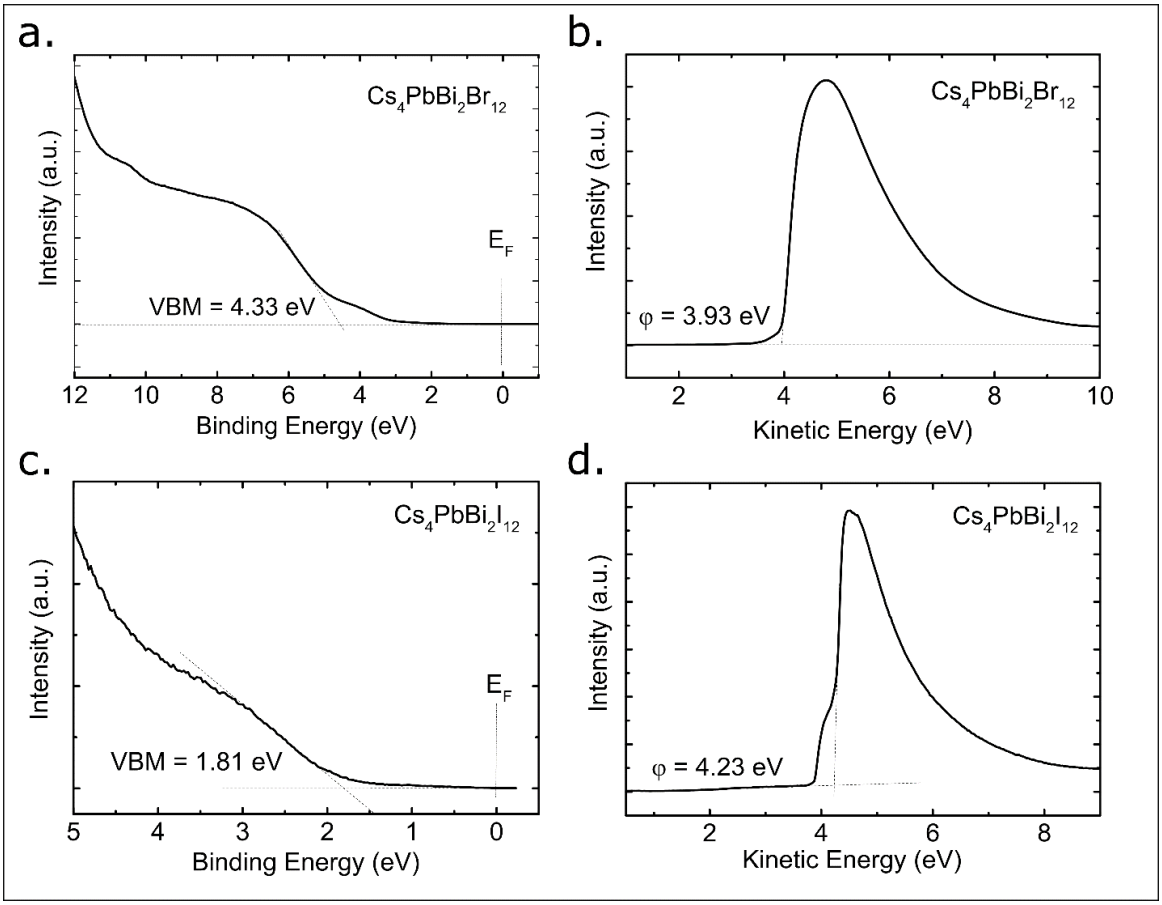

Figure S3. Ultraviolet photoelectron spectroscopy (UPS) for the double perovskites. a) binding energy and b) kinetic energy spectrum for $Cs_4PbBi_2Br_{12}$. c) binding energy and d) kinetic energy spectrum for $Cs_4PbBi_2I_{12}$

Table S1. Fit parameters for the time-resolved photoluminescence decay of the double perovskites. For the fitting the following equation was used:

$$I = \sum_i a_i e^{-\frac{t-t_0}{\tau_i}}$$

where A_i is the percentile contribution of the decay ($a_i/\Sigma a_i$) and τ_i is the decay time and τ_{avg} is the average decay time.

	A_1	τ_1	A_2	τ_2	A_3	τ_3	$\boldsymbol{\tau_{avg}}$
Compound	(%)	(ns)	(%)	(ns)	(%)	(ns)	**(ns)**
$Cs_4PbBi_2Br_{12}$	66.5	1.97	33.50	6.41	-	-	**4.1**
$Cs_4PbBi_2I_{12}$	74.4	0.19	23.7	0.56	0.07	3.81	**0.39**

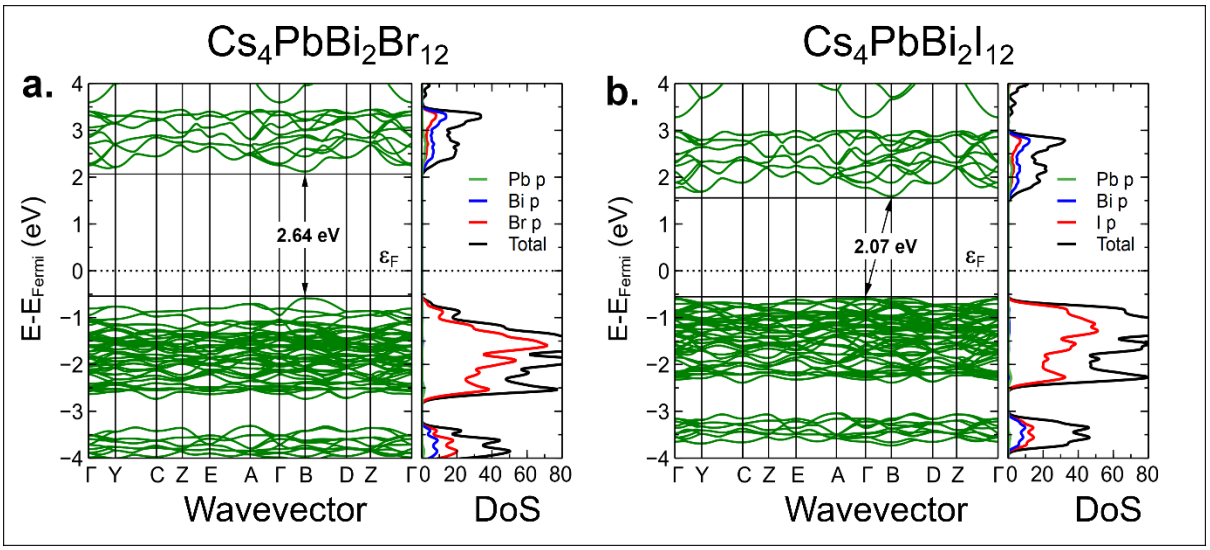

Figure S4. Band structure and projected DoS of monoclinic structures of a) $Cs_4PbBi_2Br_{12}$ and b) $Cs_4PbBi_2I_{12}$.

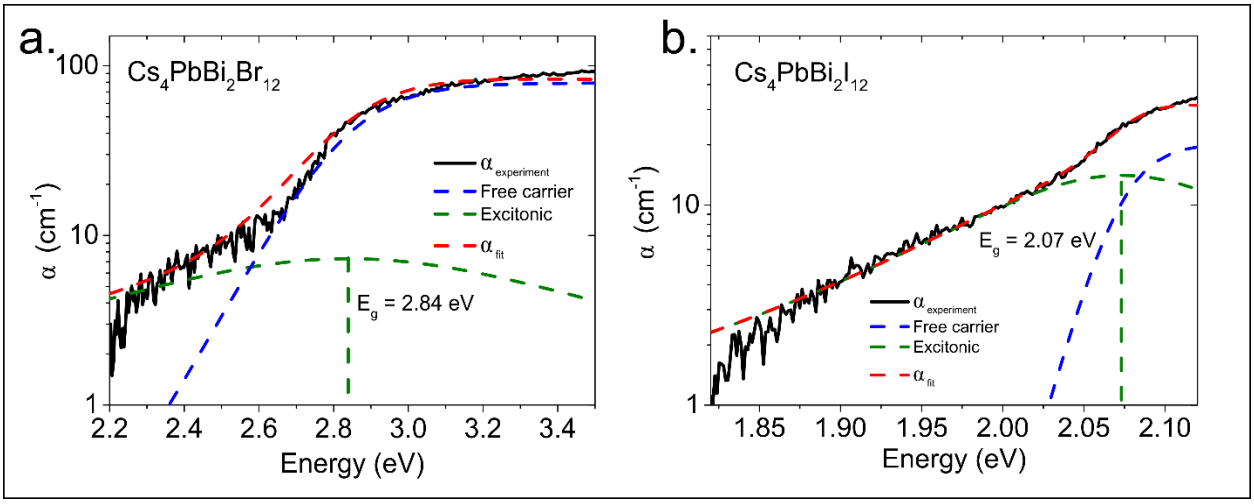

Figure S5. Fit of the absorption spectra with Elliot formalism to determine the bandgap for a) $Cs_4PbBi_2Br_{12}$ and b) $Cs_4PbBi_2I_{12}$.

Fitting of absorption curves. The fit was performed by using Elliot formalism.[1] Here, the contributions to the absorption coefficient (α) can be defined from free carriers (continuum) (α_c) and excitons (α_{ex}).

$$\alpha(\hbar\omega) = \alpha_c + \alpha_{ex} \quad \textbf{(1)}$$

$$\alpha(\hbar\omega) = P_{cv}\left[\theta\left(\hbar\omega - E_g\right)\cdot\left(\frac{\pi e^{\pi x}}{\sinh(\pi x)}\right) + R_{ex}\sum_{n=1}^{\infty}\frac{4\pi}{n^3}\cdot\delta\left(\hbar\omega - E_g + \frac{R_{ex}}{n^2}\right)\right] \quad \textbf{(2)}$$

with:

$$x = \sqrt{R_{ex}/(\hbar\omega - E_g)} \quad \textbf{(3)}$$

where P_{cv} is approximated as a constant related to the interband transition matrix element, $\hbar\omega$ is the photon energy, $\theta(\hbar\omega\text{-}E_g)$ is the Heaveside step function, R_{ex} is the Rydberg energy, n is the principle quantum number, and δ is the delta function.

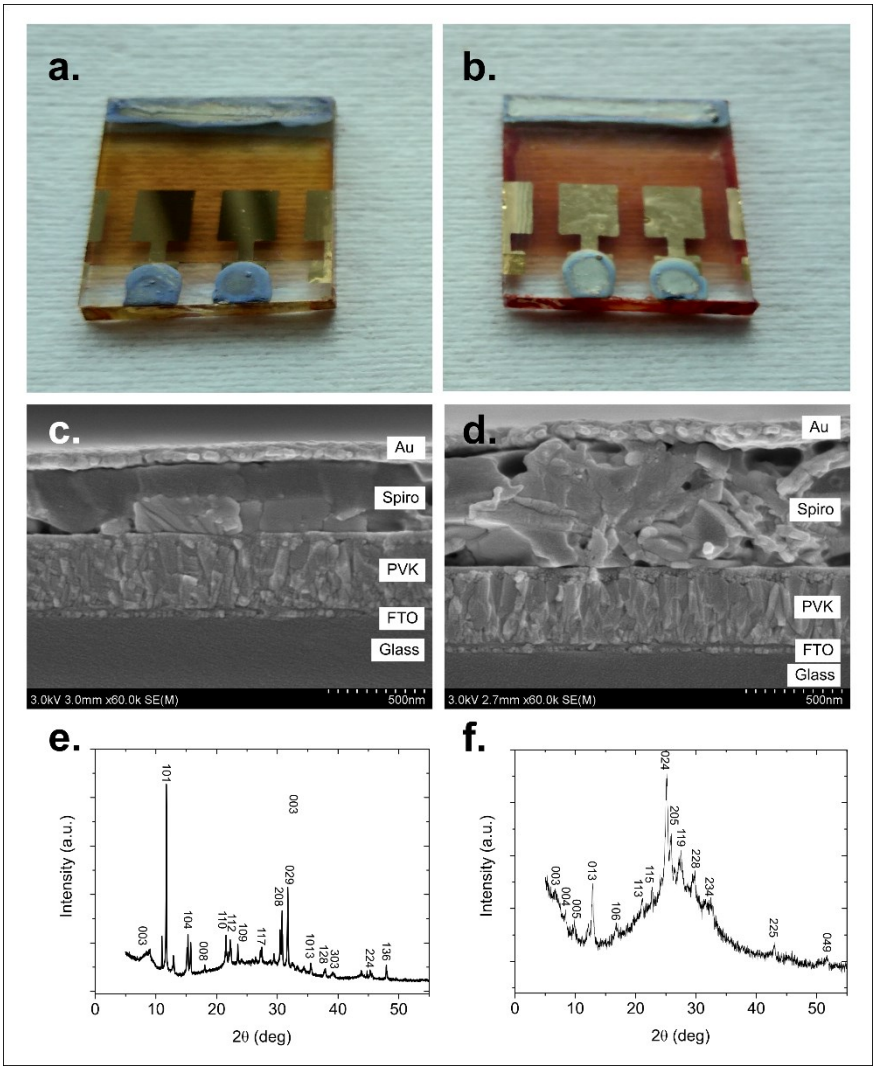

Figure S6. Picture of the photodiodes used in the electrical measurements. a) $Cs_4PbBi_2Br_{12}$ diode, and b) $Cs_4PbBi_2I_{12}$ diode. Scanning electron microscope images of the cross-section of the c) $Cs_4PbBi_2Br_{12}$ diode, and d) $Cs_4PbBi_2I_{12}$ diodes (Spiro: Spiro-OMeTAD; PVK: Perovskite). We notice that the Spiro-OMeTAD layer in the I-variant of the device is thicker than for the Br-variant, however the conductivity is high enough that we do not expect it will significantly impact the performance of the device. X-ray diffraction of the films used in the e) $Cs_4PbBi_2Br_{12}$ diode, and f) $Cs_4PbBi_2I_{12}$ diode. The XRD profiles of the films (Suppl. Figure S1) and the single crystals present the same peaks as expected, however due to different preferred orientation the intensities of the different peaks differ, since some reflection will be preferred.

Table S2. Fit parameters for the (negative) thermal quenching of the scintillation intensity of the perovskites.

	C_1	E_1	C_2	E_2	D	E'_1
Compound	(-)	(meV)	(-)	(meV)	(-)	(meV)
$Cs_4PbBi_2Br_{12}$	1.16	3.77	450	78.9	81.2	53.3
$Cs_4PbBi_2I_{12}$	2.71×10^3	29.7	0	-	0	-

The fit was carried out according to the model proposed by Shibata et al.:[2]

$$||I(T)|| = \frac{1+D\cdot e^{-E'_1/k_BT}}{1+C_1\cdot e^{-E_1/k_BT}+C_2\cdot e^{-E_2/k_BT}} \quad \textbf{(4)}$$

where D is the negative thermal quenching coefficient which describes the contribution from thermally excited electrons, C_1 and C_2 are the thermal quenching coefficients related to non-radiative electron excitation leading to thermal quenching, E'_1 is the activation energies for negative thermal quenching and E_1 and E_2 are the activation energies for typical thermal quenching, respectively and k_B is the Boltzmann constant. We note that for the iodide variant there is no negative thermal quenching (hence, D= 0) and thus it reduces to regular thermal quenching with one single decay (i.e. C_2= 0).

Table S3. Fit parameters of the afterglow decay at 10 K, fitted with a multiple exponential decay (see Table S1), where A_i is the percentile contribution of the decay and τ_i is the decay time and τ_{avg} is the average decay time.

	A_1	τ_1	A_2	τ_2	A_3	τ_3	τ_{avg}
Compound	(%)	(s)	(%)	(s)	(%)	(s)	**(ns)**
$Cs_4PbBi_2Br_{12}$	85.9	148	14.10	944	-	-	**282**
$Cs_4PbBi_2I_{12}$	45.4	9.82	43.2	67.3	11.4	399	**84.5**

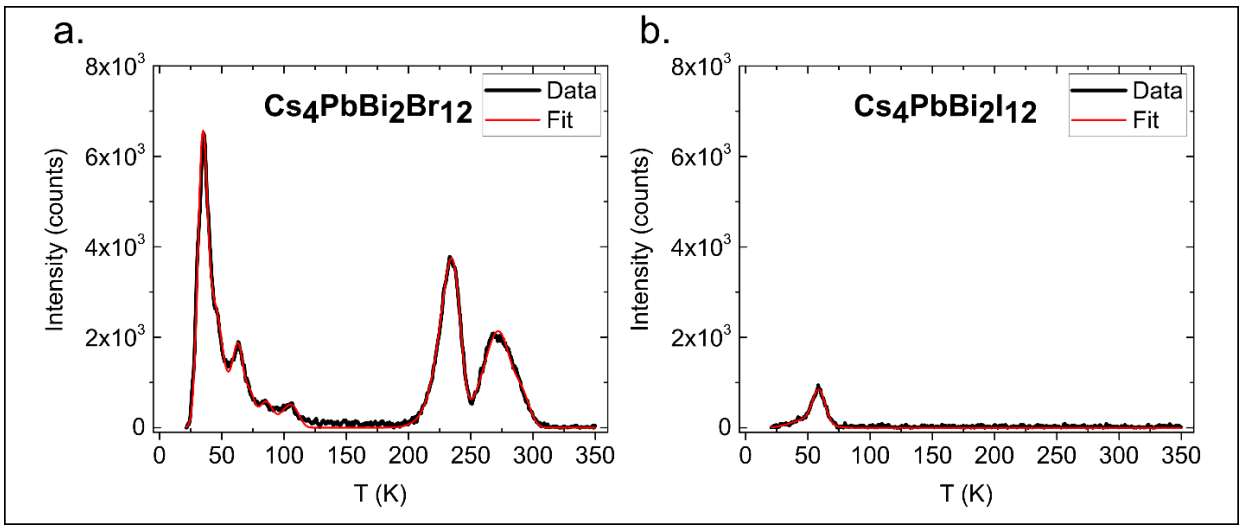

Figure S7. Thermoluminescence peaks for $Cs_4PbBi_2Br_{12}$ and b) $Cs_4PbBi_2I_{12}$ with corresponding fits.

Thermoluminescence peaks fit. The fit was carried out with the starting assumption that the traps in the thermoluminescence spectra can be represented as quasi-continuous trap distributions. We use the procedure described by Brylew et al.[3] to determine the trap parameters:

$$I_{TL} = \sum_{i=1}^{k} n_0 V \sigma_i \cdot \exp\left(-\frac{E_i}{k_B T}\right) \cdot \exp\left(-\frac{\sigma_i}{\beta}\int_{T_0}^{T} \exp\left(-\frac{E_i}{k_B T'}\right) dT'\right) \qquad \textbf{(5)}$$

where $T_0 \approx 0$ K, E_i is the trap depth, β is the heating rate (0.15 K·s^{-1}), V is the crystal volume, n_0 is the trap concentration, and a value of 10^{12} s^{-1} was used for the frequency factor, σ_i, for all fittings.

The parameters for the fit are presented in Table S4, below. T_m is the temperature of the glow peak maximum.

Table S4. Parameters of the thermoluminescence peak fitting.

	T_m	E	n_0
Compound	(K)	(meV)	(a.u.)
$Cs_4PbBi_2Br_{12}$	34	68.2	1.85×10^4
	44	84.8	9.31×10^3
	62	95.5	8.29×10^3
	71	126	9.42×10^3
	85	195	5.56×10^4
	105	252	3.90×10^4
	234	572	7.74×10^4
	270	615	4.34×10^4
	286	666	2.72×10^4
$Cs_4PbBi_2I_{12}$	49	279	5.76×10^3
	59	335	8.91×10^3

References

1. Elliott, R. J., Intensity of Optical Absorption by Excitons. *Phys. Rev.* **1957,** *108* (6), 1384-1389.
2. Shibata, H., Negative Thermal Quenching Curves in Photoluminescence of Solids. *Jpn. J. Appl. Phys* **1998,** *37* (Part 1, No. 2), 550-553.
3. Brylew, K.; Drozdowski, W.; Wojtowicz, A. J.; Kamada, K.; Yoshikawa, A., Studies of low temperature thermoluminescence of GAGG:Ce and LuAG:Pr scintillator crystals using the Tmax–Tstop method. *J. Lumin.* **2014,** *154*, 452-457.